Electronic Supplementary Material (ESI) for Journal of Materials Chemistry C.

Supporting Information

Insight into In-Plane Isotropic Transport in Anthracene-Based Organic Semiconductors

Xingwei Zeng,[a] Dongwei Zhang,*[b] Yanan Zhu,[a] Mo Chen,[a] Haibiao Chen,[a] Seiya Kasai,[c] Hong Meng,*[a] and Osamu Goto*[a]

[a] *School of Advanced Materials, Peking University Shenzhen Graduate School, Peking University, Shenzhen 518055, China*
[b] *The Institute for Solid State Physics, The University of Tokyo, 5-1-5 Kashiwanoha, Kashiwa, Chiba 277-8581, Japan*
[c] *Research Center for Integrated Quantum Electronics, Hokkaido University, North 13, West 8, Sapporo 060-0813, Japan*

Contents

1. Calculated Anisotropy Ratio and Related Parameters for Three Series of Anthracene Derivatives

Table S1. Calculated anisotropy ratio and related parameters for 9,10-ANTs

#	Name	Structure	Packing	i	r_i/Å	θ_i/°	γ_i/°	V_i (meV)	λ(eV)	μ_{max}/μ_{min}
1	9,10-DPAnt	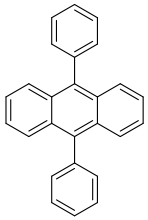	Slipped Herringbone	P_1	8.628	0	38.2	1.01	0.265	3.08
				T_1	9.136	42.1	0	4.54		
				T_2	8.092	84.7	42.3	3.76		
				T_3	9.136	137.9	0	4.54		
				P_2	8.628	180.0	38.2	29.48		
				T_4	9.136	222.1	0	4.54		
				T_5	8.167	261.3	41.8	22.45		
				T_6	9.136	317.9	0	4.54		
2	BPEAnt	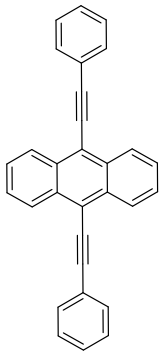	Slipped Herringbone	P_1	5.357	0	0	42.39	0.145	1.04×10^4
				T_1	13.299	54.6	69.7	4.96		
				T_2	13.299	124.1	69.0	4.76		
				T_3	15.305	152.8	53.8	0.06		
				P_2	5.357	180.0	0	42.39		
				T_4	10.018	227.3	38.0	0.7		
				T_5	8.465	270.0	47.3	2.44		
				T_6	10.018	313.3	38.8	0.7		

#	Name	Structure	Packing	i	r_i/Å	θ_i/°	γ_i/°	V_i (meV)	λ(eV)	μ_{max}/μ_{min}
3	BNEAnt	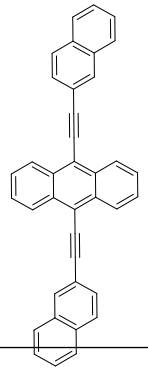	Slipped Herringbone	P_1	5.957	0	0	13.77	0.146	7.46
				T_1	18.16	27.4	54.7	0.2		
				T_2	16.088	54.4	71.4	0.06		
				T_3	16.088	128.8	72.8	0.06		
				P_2	5.957	180.0	0	13.77		
				T_4	9.639	238.4	53.9	8.88		
				T_5	9.639	278.8	52.7	8.87		
				T_6	12.801	339.3	34.0	0.01		

Table S2. Calculated anisotropy ratio and related parameters for 2-ANTs

#	Name	-R=	Packing	i	r_i/Å	θ_i/°	γi/°	V_i(meV)	λ(eV)	μ_{max}/μ_{min}
4	NaAnt	-R= 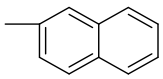	Layered Herringbone	P_1	6.019	0	0	10.3	0.174	20.4
				T_1	5.057	53.48		4.14		
				T_2	5.057	126.52		4.15		
				P_2	6.019	180		10.3		
				T_3	5.117	233.97		5.33		
				T_4	5.117	306.03		5.65		
5	2Ant	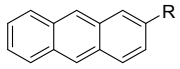 -R= 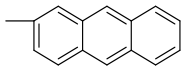	Layered Herringbone	P_1	5.957	0	0	27.04	0.104	1.82
				T_1	4.805	51.34		42.44		
				T_2	4.777	128.22		40.53		
				P_2	5.957	180		27.04		
				T_3	4.748	231.42		47.76		
				T_4	4.777	308.66		35.50		
6	FlAnt	-R= 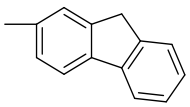	Layered Herringbone	P_1	6.049	0	0	5.94	0.185	110.5
				T_1	5.087	51.556	14.19	8.22		
				T_2	5.037	127.05	10.63	52.14		
				P_2	6.049	180	0	5.94		
				T_3	5.093	232.45	12.85	15.94		
				T_4	5.093	308.28	16.55	5.54		

Table S3. Calculated anisotropy ratio and related parameters for 2-6-ANTs

#	Name	-R=	i	r_i/Å	θ_i/°	V_i(meV)	λ(eV)	μ_{max}/μ_{min}	μ_{max}/μ_{min} (Experimental)
	Anthracene	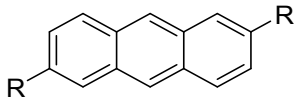 R = -H	P	6.01	0	40.40	0.138	9.55	--
			T_1	5.22	54.9	23.23			
			T_2	5.22	125.1	23.23			
7a	DTAnt	R= 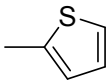	P	6.09	0	9.65	0.261	1.50	--
			T_1	4.835	51.0	39.78			
			T_2	4.835	129.0	39.78			
7b	DHTAnt	R = 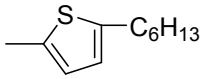	P	5.866	0	20.61	0.313	1.09	--
			T_1	4.72	51.6	29.75			
			T_2	4.72	128.4	29.75			
8a	DPVAnt	R = 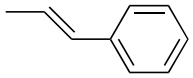	1	5.888	0	36.3	0.166	1.12	1.5-1.95
			2	4.695	51.5	52.07			
			3	4.718	128.9	57.42			
			4	5.888	180.0	36.3			
			5	4.718	231.1	57.42			
			6	4.695	308.5	52.07			

#	Name	-R=	i	r_i/Å	θ_i/°	V_i(meV)	λ(eV)	μ_{max}/μ_{min}	μ_{max}/μ_{min} (Experimental)
8b	DPPVAnt	R = 	P	5.848	0	32.08	0.181	1.3	--
			T_1	4.65	51.0	59.36			
			T_2	4.65	129.0	59.36			
9	o-DPyAnt	R = 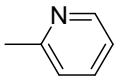	P	6.235	0	31.38	0.155	1.32	--
			T_1	4.816	49.7	78.98			
			T_2	4.816	130.3	78.91			
10	DPA	R = 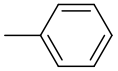	P	6.245	0	10.01	0.176	1.38	1.3-1.5
			T_1	4.823	49.6	56.97			
			T_2	4.823	130.4	56.97			
11	BEPAnt	R = 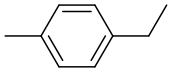	P	6.04	0	20.53	0.179	1.4	1.3-2.0
			T_1	4.9	51.9	38.47			
			T_2	4.9	128.1	38.47			
12	BOPAnt	R = 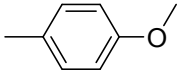	P	6.16	0	10.91	0.249	1.49	1.2
			T_1	4.83	50.4	33.74			
			T_2	4.83	129.6	33.74			

#	Name	-R=	i	r_i/Å	θ_i/°	V_i(meV)	λ(eV)	μ_{max}/μ_{min}	μ_{max}/μ_{min} (Experimental)
13	BDBFAnt	R = 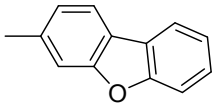	P	5.98	0	18.43	0.166	1.32	1.2-1.3
			T_1	4.79	51.4	33.56			
			T_2	4.79	128.6	33.56			

* Experimental results of single-crystal OFETs.

2. The Molecular Packing Architecture Parameter θ_i and The Calculated Electronic Property Parameter V_i for 2,6-ANTs, 9,10-ANTs, and 2-ANTs

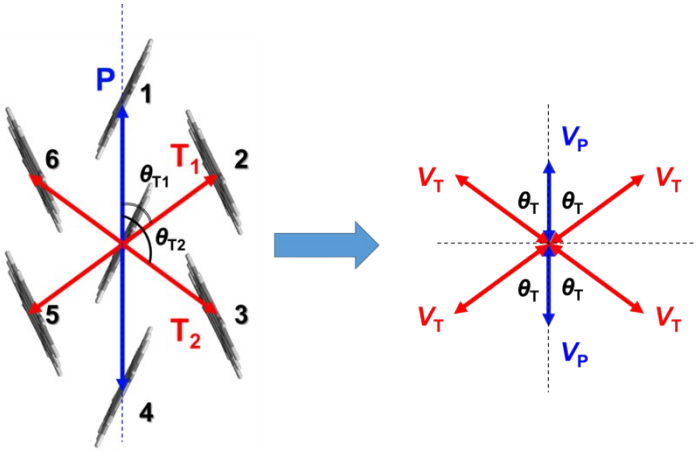

Figure S1. Layered-herringbone (LHB) packing with molecules arranged symmetrically with respect to a line along the parallel (π-π stacking) direction satisfies $r_{T1} \approx r_{T2}$, $\theta_{T2} \approx \pi - \theta_{T1}$. In this case, the molecular arrangement is symmetrical with respect to both directions parallel and perpendicular to the π-π stacking direction. The dual symmetry results in equal transfer integrals, i.e., $V_{T1} \approx V_{T2}$. 2,6-ANTs satisfy these conditions including the material #**8a**.

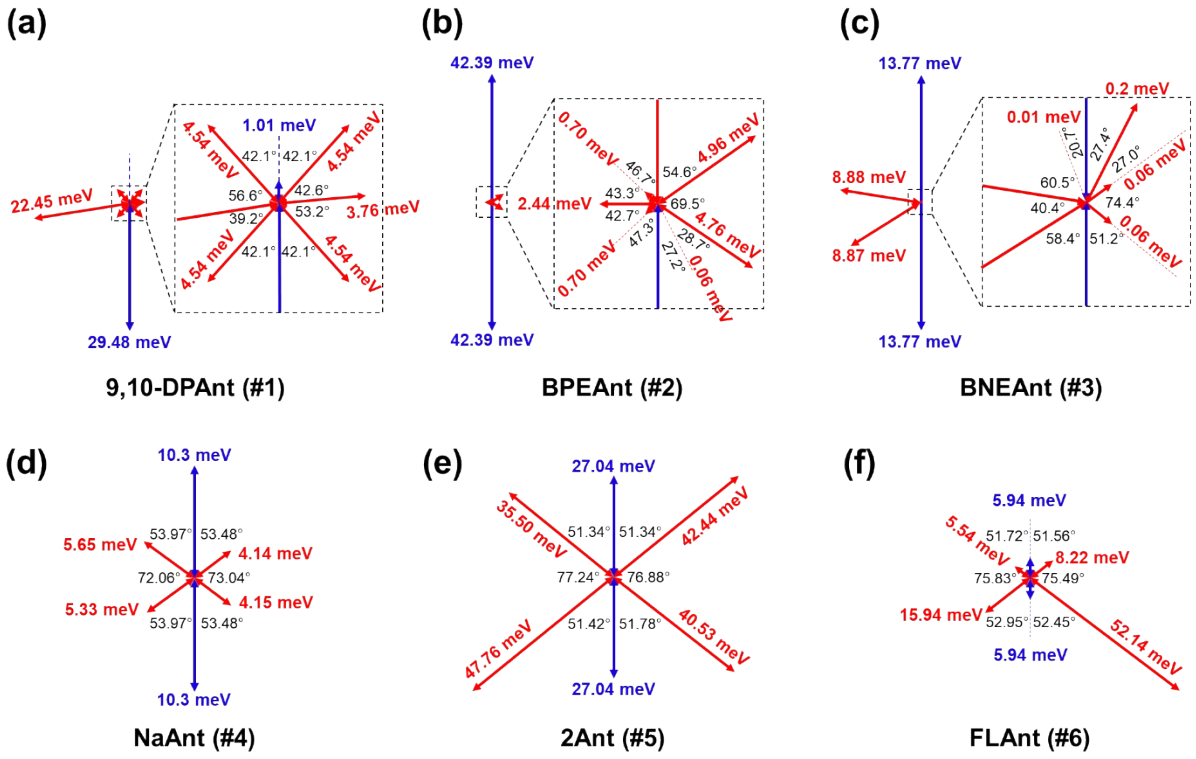

Figure S2. The molecular packing architecture parameter θ_i and the calculated electronic property parameter V_i for (a)-(c) 9,10-ANTs and for (d)-(f) 2-ANTs.

3. Summary of Reported Mobility for Three Series of Anthracene Derivatives

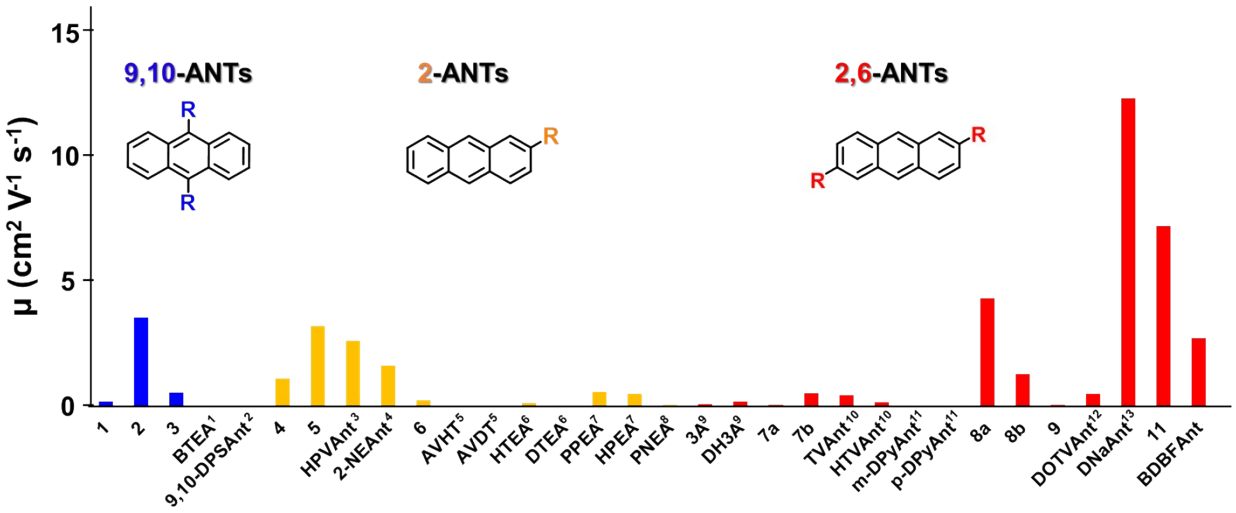

Figure S3. Reported field-effect hole mobility for three series of anthracene derivatives. The data for 9,10-ANTs, 2-ANTs, and 2,6-ANTs are colored in blue, yellow, and red, respectively.

4. Intermolecular Distance and Torsion Angle for 2,6-ANTs

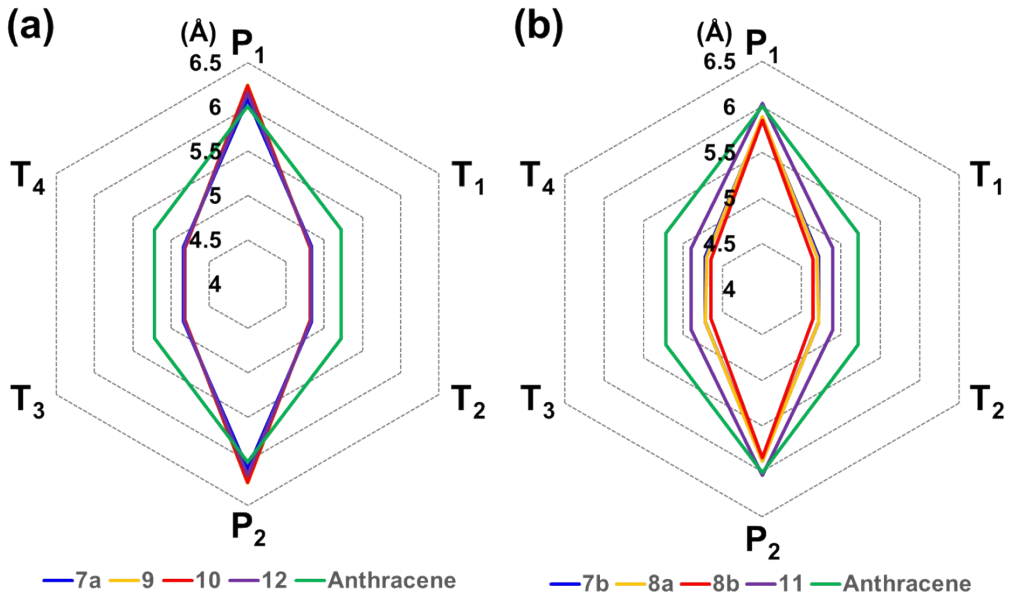

Figure S4. Intermolecular distances between the centroids of neighboring molecules in 2,6-ANTs for (a) datasets of blue dots and (b) those of black dots in **Figure 3**.

Table S4. List of torsion angles between the central anthracene ring and side group obtained from single-crystal data of 2,6-ANTs.

#	Name	Torsion Angle (°)
8b	DPPVAnt	2.13
8a	DPVAnt	3.26
7b	DHTAnt	5.54
7a	DTAnt	10.71
11	BEPAnt	11.38
12	BOPAnt	15.61
10	DPA	20.33
9	o-DPyAnt	28.52

5. Crystal Structure of BDBFAnt

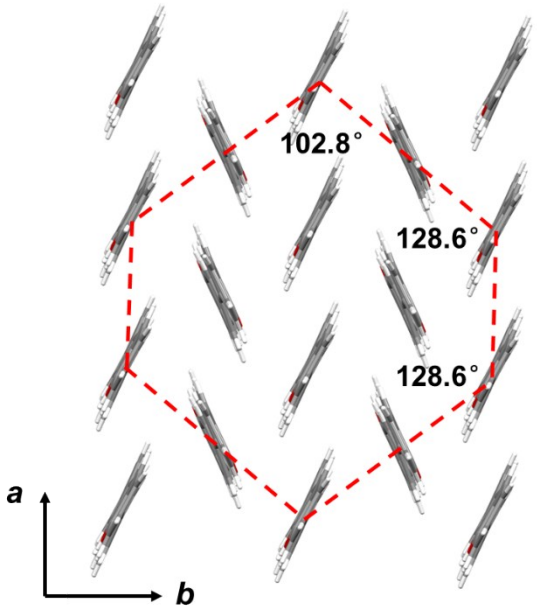

Figure S5. Facet angles of BDBFAnt within the basal packing plain.

6. Field Effect Mobility of BDBFAnt SC-OFETs by Considering Series Resistance

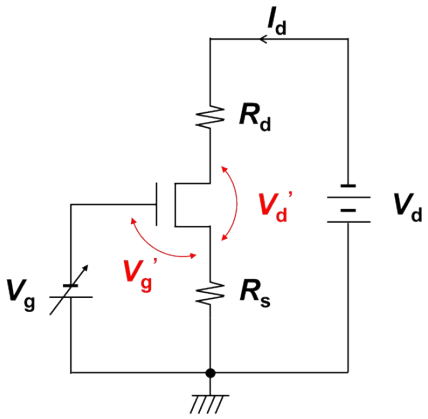

$$V_g' = V_g - R_s I_d$$

$$V_d' = V_d - (R_d + R_s) I_d$$

$$I_d = K\left\{(V_g' - V_{th})V_d' - \frac{1}{2}V_d'^2\right\}$$

$$K = \mu C_i \frac{L}{W}$$

μ: field effect mobility,
C_i: gate capacitance,
L: gate length, W: gate width

$$R_s = R_d = R_{sd}$$

Linear region

$$I_d = \frac{K(V_g - V_{th} - \frac{1}{2}V_d)V_d}{1 + KR_{sd}\{2(V_g - V_{th}) - V_d\}}$$

Saturation region

$$I_d = \frac{KR_{sd}(V_g - V_{th}) + 1 - \sqrt{2KR_{sd}(V_g - V_{th}) + 1}}{KR_{sd}^2}$$

Figure S6. Equivalent circuit of BDBFAnt SC-OFET by taking account of series resistances in source and drain sides, R_s and R_d, respectively. Formulas are derived under the assumption of $R_s = R_d = R_{sd}$.

Table S5. Summary of fitting results with and without considering series resistance R_{sd}. S is the total area of the source and drain contacts, d is the thickness of the single crystal, ρ is resistivity, and n is carrier concentration in the active layer at $V_g = V_{th} - 10$ V, respectively.

a) Large crystal

						Considering series resistance R_{sd}					Without considering R_{sd}	
OFET No.	W (μm)	L (μm)	S (cm^2)	d (cm)	Vg	Vth (V)	μ (cm^{-2} V^{-1} s^{-1})	R_{sd} (kΩ)	ρ (Ωcm)	n@V_{th} - 10 (V) (cm^{-3})	Vth (V)	μ (cm^{-2} V^{-1} s^{-1})
1	260	42	6.1E-08	4.5E-08	Forward	-38.3	2.7	30	4.1E+04	5.7E+13	-38.3	2.5
					Reverse	-42.8	3.3			4.6E+13	-42.8	2.7
2	202	42	5.3E-08	4.5E-08	F	-37.8	2.5	120	1.4E+05	1.8E+13	-37.8	2.0
					R	-42.5	3.2			1.4E+13	-42.5	2.3
3	205	39	4.8E-08	4.5E-08	F	-47.5	2.4	70	7.4E+04	3.5E+13	-47.5	2.0
					R	-50.6	2.9			2.9E+13	-50.6	2.3
4	178	40	4.0E-08	4.5E-08	F	-42.5	1.9	80	7.1E+04	4.6E+13	-42.5	1.5
					R	-47.9	2.6			3.4E+13	-47.9	2.0
5	133	42	2.7E-08	4.5E-08	F	-43.6	2.3	110	6.6E+04	4.1E+13	-43.6	1.9
					R	-49.4	3.3			2.9E+13	-49.4	2.5

b) Small crystals

						Considering series resistance R_{sd}					Without considering R_{sd}	
OFET No.	W (μm)	L (μm)	S (cm^2)	d (cm)	Vg	Vth (V)	μ (cm^{-2} V^{-1} s^{-1})	R_{sd} (kΩ)	ρ (Ωcm)	n@V_{th} - 10 (V) (cm^{-3})	Vth (V)	μ (cm^{-2} V^{-1} s^{-1})
1	196	43	4.0E-08	6.0E-08	Forward	-37.3	2.6	320	2.1E+05	1.1E+13	-37.3	1.7
					Reverse	-40.3	2.8			1.0E+13	-40.3	1.8
2	189	46	2.2E-08	4.0E-08	F	-26	2.5	380	2.1E+05	1.2E+13	-26.0	1.7
					R	-31.3	3.0			9.9E+12	-31.3	1.7
3	304	29	8.0E-08	4.5E-08	F	-45.9	2.7	120	2.1E+05	1.1E+13	-45.9	1.8
					R	-46.5	3.0			9.8E+12	-46.5	1.9
4	193	50	1.7E-08	5.3E-08	F	-44.9	2.7	190	6.1E+04	3.8E+13	-44.9	2.2
					R	-49.2	3.4			3.0E+13	-49.2	2.3

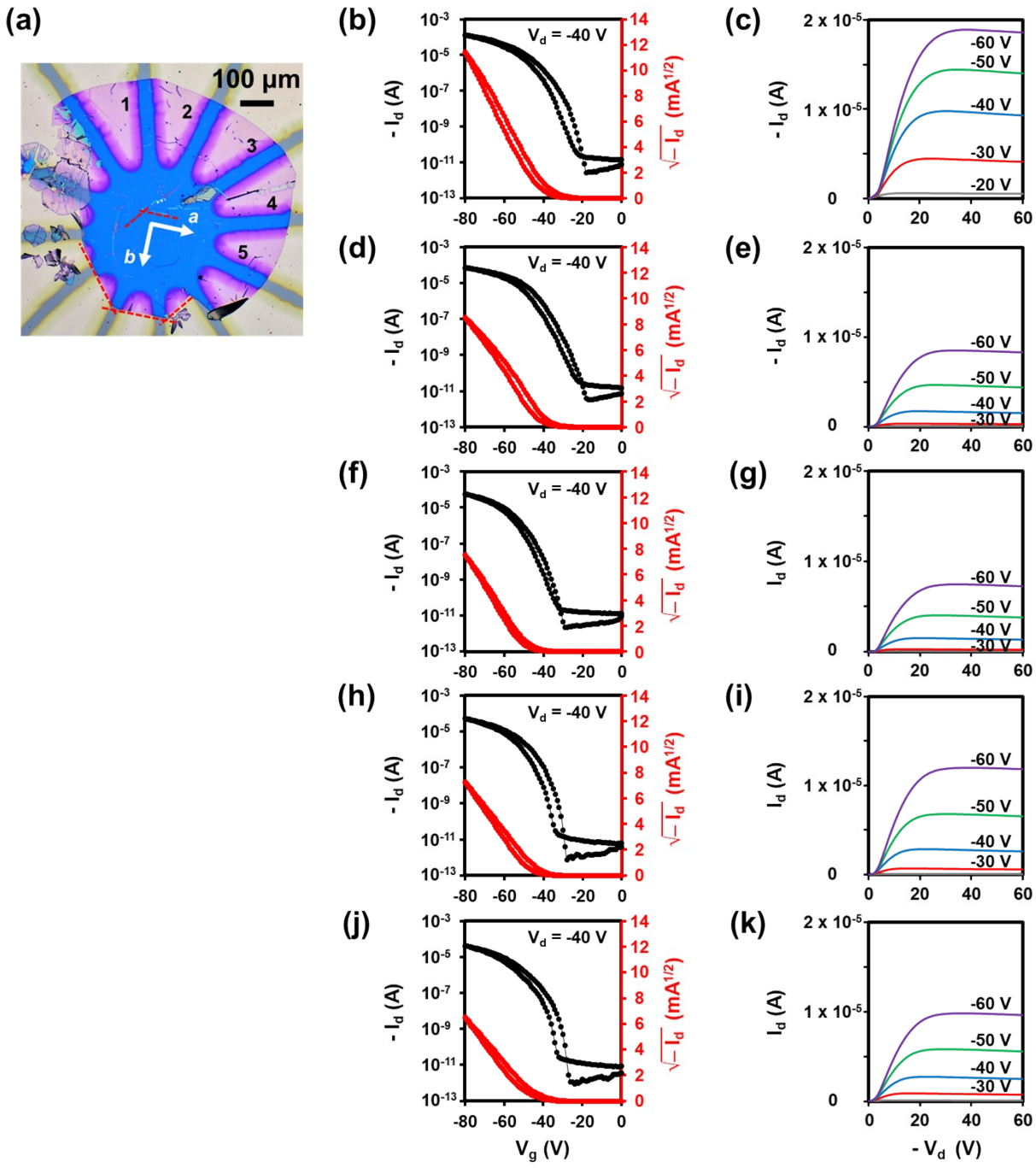

Figure S7. (a) Micrograph of the fabricated fan-shaped SC-OFET device. Five SC-OFETs (#1 - #5) were obtained. (b), (d), (f), (h), (j) Transfer curve ($I_d - V_g$) for each SC-OFET #1 - #5, respectively. Transfer curves were obtained in the saturation region (V_d = -40 V) after three consecutive measurements. (c), (e), (g), (i), (k) Output curve ($I_d - V_d$) for each SC-OFET #1 - #5, respectively. Each $I_d - V_d$ curve was taken before measuring transfer curve; we observed a transient response in measuring $I_d - V_d$, i.e., holes in the active layer were captured by interface traps between organic semiconductor and OTS-modified SiO_2 layer.

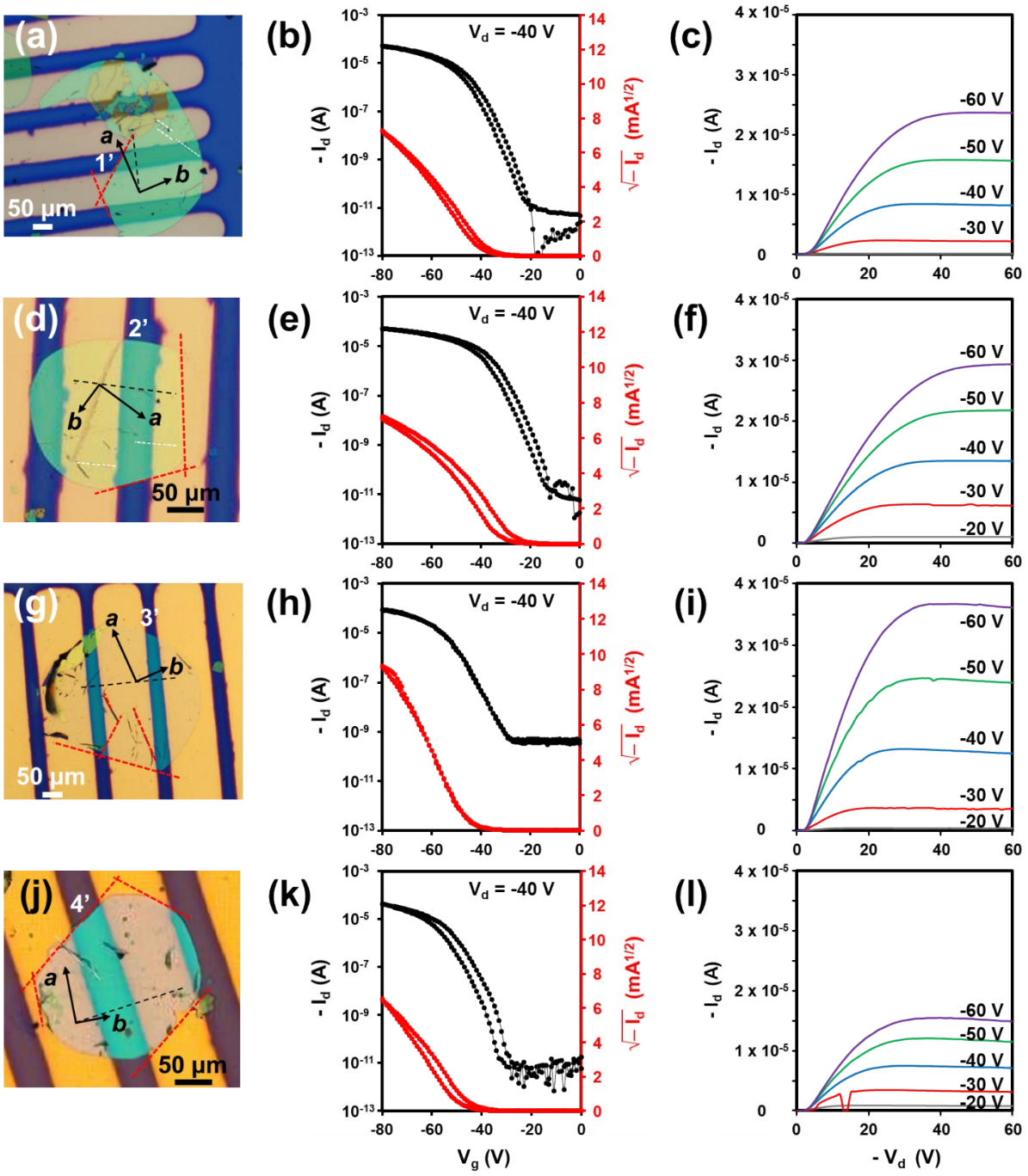

Figure S8. (a), (d), (g), (j) Micrographs of the fabricated SC-OFETs. Four SC-OFETs (#1' - #4') were shown. (b), (e), (h), (k) Transfer curve ($I_d - V_g$) for each SC-OFET #1' - #4', respectively. Transfer curves were obtained in the saturation region (V_d = -40 V) after three consecutive measurements. (c), (f), (i), (l) Output curve ($I_d - V_d$) for each SC-OFET #1' - #4', respectively. Each $I_d - V_d$ curve was taken before measuring transfer curve; we observed a transient response in measuring $I_d - V_d$, i.e., holes in the active layer were captured by interface traps between organic semiconductor and OTS-modified SiO_2 layer.

6. Theoretical Methodology in Details

A model combining Marcus-Hush theory with first-principle quantum mechanics is developed for the analysis in this work.[14, 15] The hopping events are considered as irrelevant from each other. Besides, homogeneous random walk is assumed for the charge motion between molecules. Thereby, the diffusion coefficient between molecules based on the hopping rate could be derived as

$$D = \lim_{t\to\infty} \frac{1}{2n} \frac{\langle x(t^2)\rangle}{t} \approx \frac{1}{2n}\sum_i r_i^2 W_i P_i \quad , \tag{1}$$

where n is the spatial dimensionality of the system, r_i is the distance between two molecules, P_i is the relative probability of the charge transfer in ith dimer and W_i is the charge transfer rate of the ith dimer. Meantime, W_i calculated from Marcus-Hush equation can be obtained as follows,

$$W_i = \frac{V^2}{\hbar}\left(\frac{\pi}{\lambda k_B T}\right)^{\frac{1}{2}} \exp\left(-\frac{\lambda}{4k_B T}\right) . \tag{2}$$

Here, V is the transfer integral between two neighboring molecules and λ is the reorganization energy, k_B is the Boltzmann constant, T is absolute temperature.

Hopping probability P_i is calculated from the following equation

$$P_i = \frac{W_i}{\sum W_i} . \tag{3}$$

The hopping mobility (μ) is obtained from Einstein's equation as follows,

$$\mu = \frac{e}{k_B T} D = \frac{e}{k_B T} \frac{1}{2n}\sum_i r_i^2 W_i P_i \quad , \tag{4}$$

where e is unit charge. In order to evaluate in-plane mobility anisotropy, a further derivation is necessary for equation (4). Wen *et al.* analyzed the mobility of components for each surface in terms of angles of the hopping jumps (γ_i) between adjacent molecules relative to the plane of interest ($Vr_i \cos\gamma_i$). According to their consideration, the transfer mobility ($\mu(\varphi)$) can be obtained as follows,

$$\mu(\varphi) = \frac{e}{k_B T} \frac{1}{2n}\sum_i \left[r_i \cos\gamma_i \cos\left(\theta_i - \varphi\right)\right]^2 W_i P_i = \sum_i \mu_i \cos^2\gamma_i \cos^2\left(\theta_i - \varphi\right) \quad , \tag{5}$$

where $r_i \cos\gamma_i \cos\left(\theta_i - \varphi\right)$ is the projection of the hopping path on the transistor channel, μ_i is the individual mobility on each charge hopping path, γ_i is the angle between the each charge hopping path and the plane of interest. **Figure 1**a schematically shows the hopping paths and angles for the herringbone packing monolayer. Three types of hopping paths including parallel (P), transverse type 1 (T1) and type 2 (T2) and the angles (θ_{T1} and θ_{T2}) between P and T1(or T2) contacts are labelled. The orientation angle (φ) of the transistor channel is defined as the base of b-axis (the parallel direction).

In order to analyze the carrier transport anisotropy of organic semiconductors, we need the maximum and the minimum of function $\mu(\varphi)$. In order to obtain these values, we simplify equation (5) to a lower order as follows,

$$\mu(\varphi) = \sum_i \frac{1}{2}\mu_i \cos^2\gamma_i \left[1 + \cos\left(2\theta_i - 2\varphi\right)\right] . \tag{6}$$

The equation could be further written as

$$\mu(\varphi) = A\cos 2\varphi + B\sin 2\varphi + C , \tag{7}$$

where factors *A*, *B*, and *C* are

$$A = \frac{1}{2}\sum_i \mu_i \cos^2 \gamma_i \cos 2\theta_i \quad , \tag{8}$$

$$B = \frac{1}{2}\sum_i \mu_i \cos^2 \gamma_i \sin 2\theta_i \quad , \tag{9}$$

$$C = \frac{1}{2}\sum_i \mu_i \cos^2 \gamma_i \quad . \tag{10}$$

Thereby, the maximum and the minimum mobility for any types of organic semiconductors can be obtained as follows,

$$\mu_{max} = C + \sqrt{A^2 + B^2} \quad , \tag{11}$$

$$\mu_{min} = C - \sqrt{A^2 + B^2} \quad . \tag{12}$$

According to these equations, we can directly calculate the mobility anisotropy ratio (μ_{max}/μ_{min}) using electronic property parameters (transfer integral *V* and reorganization energy λ) and molecular packing architecture parameters (*r*, *θ*, and *γ*) for organic semiconductors.

Organic semiconductors such as 2,6-Ants have the herringbone packing motif with a symmetric arrangement with respect to a line along the parallel (π-π stacking) direction and satisfy specific conditions, which are $r_{T1} = r_{T2}$, $\theta_{T2} = \pi - \theta_{T1}$ in **Figure 1**a, and $V_{T1} = V_{T2}$. Here, V_{T1} and V_{T2} are the transfer integrals between dimers along the T1 and T2 direction with hopping distances of r_{T1} and r_{T2}, respectively. θ_{T1} and θ_{T2} are the angles between P and T1 (or T2) directions, respectively. From geometry we can prove that $r_{T1} = r_{T2}$ and $\theta_{T2} = \pi - \theta_{T1}$ are equivalent, and they are true if the molecular arrangement is symmetrical with respect to both directions parallel and perpendicular to the π-π stacking direction. We applied these conditions to calculate the anisotropy ratio. Under these conditions, hopping paths T1, T2, and P within a dimer are exactly on the same plane (the basal stacked layer), and then γ_i is 0°. Thereby, equivalent hopping paths T1 and T2 can be simplified as T, and the reference angles θ_{T1} and θ_{T2} can be also simplified as θ_T and $\pi - \theta_T$. (see **Figure S1**). In addition, we only consider the charge mobilities of μ_P and μ_T along the P and T directions, which could be derived from transfer integral of dimers and θ_T,

$$\frac{\mu_P}{\mu_T} = \left(V_P/V_T\right)^4 \left(r_P/r_T\right)^2 = (R)^4 \left(2\cos\theta_T\right)^2 \quad , \tag{13}$$

where V_P and V_T are the transfer integrals between dimers along the P and T directions with hopping distances of r_P and r_T, respectively. R is the ratio of the transfer integrals of V_P and V_T ($R \equiv V_P/V_T$).

Therefore, we can easily identify a specific condition for factor B being equal to zero, and then factors *A*, *B*, and *C* can be simplified as

$$A = \mu_T\left[R^4\left(2\cos\theta_T\right)^2 + 2\cos 2\theta_T\right], \tag{14}$$

$$B = 0, \tag{15}$$

$$C = \mu_T\left[R^4\left(2\cos\theta_T\right)^2 + 2\right]. \tag{16}$$

A function $f(R, \theta_T)$ specific for in-depth analysis of the relationship between mobility anisotropy, transfer integral and the angle θ_T is derived as following,

$$\frac{\mu_{max}}{\mu_{min}} = \frac{C + |A|}{C - |A|} = f(R, \theta_T) = \frac{2 + R^4(2\cos\theta_T)^2 + \left|R^4(2\cos\theta_T)^2 + 2\cos 2\theta_T\right|}{2 + R^4(2\cos\theta_T)^2 - \left|R^4(2\cos\theta_T)^2 + 2\cos 2\theta_T\right|}. \quad (17)$$

For calculation of the reorganization energy (λ), adiabatic potential energy surfaces method was applied, which could be described with the following equation,

$$\lambda = \left(E_0^* - E_0\right) + \left(E_+^* - E_+\right), \quad (18)$$

where E_0 and E_+ represent the energies of the neutral and cationic species in their lowest-energy geometries, respectively; E_0^* is the energy of neutral state with the geometry of the cationic species, and E_+^* is the energy of the cationic state with the geometry of the neutral species. All geometric optimizations and energy evaluations in the process were conducted with Gaussian 09 using the B3LYP functional set and the 6-311G(d,p) basis set.

The transfer integral of each dimer (V_i) was calculated from the corresponding spatial overlap (S_{RP}), charge transfer integral (J_{RP}), site energies (H_{RR}, H_{RP}) of the dimer,

$$V_i = \frac{J_{RP} - S_{RP}(H_{RR} + H_{RP})/2}{1 - S_{RP}^2}. \quad (19)$$

Calculations of the essential parameters (S_{RP}, J_{RP}, H_{RR}, H_{RP}) were performed using fragment analysis functions implemented in Amsterdam Density Function (ADF) software pack, which adopts PW91 functional and basis set of Double-Z 2 plus polarization function (DZ2P).

6. References

1. C. Wang, Y. Liu, Z. Ji, E. Wang, R. Li, H. Jiang, Q. Tang, H. Li and W. Hu, Chem. Mater., 2009, **21**, 2840-2845.

2. A. Dadvand, W. H. Sun, A. G. Moiseev, F. Bélanger-Gariépy, F. Rosei, H. Meng and D. F. Perepichka, J. of Mater. Chem. C, 2013, **1**, 2817-2825.

3. A. Dadvand, A. G. Moiseev, K. Sawabe, W.-H. Sun, B. Djukic, I. Chung, T. Takenobu, F. Rosei and D. F. Perepichka, Angew. Chem. Int. Ed., 2012, **51**, 3837-3841.

4. X. Zhang, G. Zhao, Y. Zhen, Z. Tu, P. He, Y. Yi, H. Dong and W. Hu, J. Mater. Chem. C, 2015, **3**, 5368-5371.

5. M. J. Hwang, J. H. Park, E. B. Jeong, I. Kang, D. H. Lee, C. E. Park, O. M. Singh, H. Choi, Y.-H. Kim, Y. J. Yoon, S.-K. Kwon and S.-G. Lee, Bull. Korean Chem. Soc., 2012, **33**, 3810-3816.

6. B. Shaik, J. H. Park, T. K. An, Y. R. Noh, S. B. Yoon, C. E. Park, Y. J. Yoon, Y. H. Kim and S. G. Lee, Tetrahedron, 2013, **69**, 8191-8198.

7. J. Y. Back, T. K. An, Y. R. Cheon, H. Cha, J. Jang, Y. Kim, Y. Baek, D. S. Chung, S. K. Kwon, C. E. Park and Y. H. Kim, ACS Appl. Mater. and Interfaces, 2015, **7**, 351-358.

8. H. G. Song, Y. Kim, S.-M. Park, T. K. An, S.-K. Kwon, C. E. Park and Y.-H. Kim, Dyes and Pigments, 2016, **131**, 349-355.

9. K. Ito, T. Suzuki, Y. Sakamoto, D. Kubota, Y. Inoue, F. Sato and S. Tokito, Angew. Chem. 2003, **115**, 1191-1194.

10. M.-C. Um, J. Jang, J. Kang, J.-P. Hong, D. Y. Yoon, S. H. Lee, J.-J. Kim and J.-I. Hong, J. Mater. Chem., 2008, **18**, 2234.

11. J. Liu, W. Zhu, K. Zhou, Z. Wang, Y. Zou, Q. Meng, J. Li, Y. Zhen and W. Hu, J. Mater. Chem. C, 2016, **4**, 3621-3627.

12. J.-P. Hong, M.-C. Um, S.-R. Nam, J.-I. Hong and S. Lee, Chem. Commun., 2009, 310-312.

13. J. Li, K. Zhou, J. Liu, Y. Zhen, L. Liu, J. Zhang, H. Dong, X. Zhang, L. Jiang and W. Hu, J. Am. Chem. Soc., 2017, **139**, 17261-17264.

14. S. H. Wen, A. Li, J. Song, W. Q. Deng, K. L. Han and W. A. Goddard, J. Phys. Chem. B, 2009, **113**, 8813-8819.

15. W. Deng, L. Sun, J. Huang, S. Chai, S. Wen and K. Han, Nat. Protoc., 2015, **10**, 632-42.